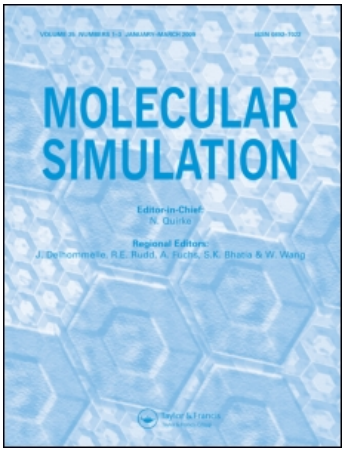

Molecular Simulation
Publication details, including instructions for authors and subscription information:
http://www.informaworld.com/smpp/title~content=t713644482

The radial breathing mode of carbon nanotubes

M. J. Longhurst[a]; N. Quirke[a]
[a] Department of Chemistry, Imperial College of Science, Technology and Medicine, South Kensington, SW, UK

To cite this Article Longhurst, M. J. and Quirke, N.(2005) 'The radial breathing mode of carbon nanotubes', Molecular Simulation, 31: 2, 135 — 141
To link to this Article: DOI: 10.1080/08927020412331308520
URL: http://dx.doi.org/10.1080/08927020412331308520

Molecular Simulation, Vol. 31, No. 2–3, 15 February–15 March 2005, 135–141

The radial breathing mode of carbon nanotubes

M.J. LONGHURST and N. QUIRKE*

Department of Chemistry, Imperial College of Science, Technology and Medicine, South Kensington, SW7 2AY UK

(Received April 2004; in final form May 2004)

We report an extensive set of results for the radial breathing modes (RBM) of infinite and finite length single walled carbon nanotubes using the second generation reactive empirical bond order potential (REBO) developed by Brenner *et al.* As expected, the frequency, ν of the RBM is inversely proportional to the nanotube radius, R_0, $\nu = \alpha/R_0$. We find two different linear fits to the data, one for zigzag tubes (3.25 THz nm) and one for armchair tubes ($\alpha = 3.18$ THz nm). For finite tubes, the RBM rapidly approaches the infinite length value for nanotubes greater than 5 nm in length.

Keywords: Reactive empirical bond order potential; Radial breathing mode

1. Introduction

In the decade since they were discovered, carbon nanotubes have attracted a great deal of attention. Advances in their chemistry have led to methods for synthesis in bulk quantities [1,2] and purification [3], and to methods for opening their sealed ends [4]. Their precisely defined geometry, strength and stability make them suitable materials for use as components of future nanotechnology. Our own interest is the use of nanotubes as nanofluidic devices. Possible applications in this area include nano-scale chemical reactors, chemical or biological sensors [5], electro-wetting [6], electrochemistry [7], and for heat transport and cooling. We have recently described the flow of wetting fluids into finite sized single wall nanotubes and explored in detail their surface properties [8,36]. A recent review [9] provides an overview of simulation work on thermomechanical and transport properties of carbon nanotubes.

A key concern in developing applications is to be able to separate nanotubes according to their chirality [10]. This in turn requires accurate means of characterisation, one such method is the use of Raman spectroscopy to detect radial breathing modes (RBM), which are strongly radius dependent. The dynamical properties of single wall carbon nanotubes have been studied and classified previously, both experimentally using resonant Raman scattering [11–16], and IR reflection spectroscopy [17], and theoretically using *ab initio* density functional methods [18,19], semiempirical tight-binding molecular dynamics [20–26], and empirical force-constant methods [24,27]. We are particularly interested in the interplay between tube dynamics and fluid flow. First principles molecular dynamics simulations with system sizes required to study fluid transport in SWNT are computationally highly demanding. An alternative is to use methods based on empirical potentials. Various ways of building an empirical many-body potential to use in condensed matter simulations have been reviewed recently [28]. Among them, an approach based on a bond-order concept [29] is particularly promising. The empirical potential of Tersoff [30–32] in the form suggested for carbon by Brenner [33] (potential I in his paper) has been widely used.

The Brenner potential has been employed by our group to calculate the phonon modes [34], and surface friction characteristics [35–37] of carbon nanotubes. However, recently a more accurate version has been available, the second-generation reactive empirical bond order (REBO) potential for hydrocarbons [38]. This new potential has been successful in modelling many different physical properties of carbon nanotubes [39–43]. In the following, we use the REBO potential to create model carbon nanotubes (both infinite and for the first time, finite

*Corresponding author. Email: n.quirke@imperial.ac.uk

Molecular Simulation
ISSN 0892-7022 print/ISSN 1029-0435 online © 2005 Taylor & Francis Group Ltd
http://www.tandf.co.uk/journals
DOI: 10.1080/08927020412331308520

length H-terminated tubes) and use molecular dynamics to characterise their RBM. We compare our results to previous theoretical [34,18,19,25,26] and experimental studies [44,45].

2. The model and simulation details

We use the second generation REBO developed by Brenner *et al.* [38]. This potential is based on the bond-order concept and implicitly contains many-body terms. It was designed to be highly transferable and has proven to be reasonably accurate in describing structural and elastic properties of carbon in difference bonding environments such as diamond, graphite and hydrocarbons. This "second-generation" potential includes both modified analytic functions for the intramolecular interactions and an expanded fitting database as compared to the original, leading to a much improved description of bond energies, lengths and C—C bond force constants.

The bond energy in this model is given by the apparently pairwise form

$$E_b(r_{ij}) = V_R(r_{ij}) - \bar{b}_{ij} V_A(r_{ij}) \tag{1}$$

where

$$V_R(r_{ij}) = (1 + Q/r_{ij}) A e^{-\alpha r_{ij}} \tag{2}$$

and

$$V_A(r_{ij}) = \sum_{n=1,3} B_n e^{-\beta_n r_{ij}} \tag{3}$$

and r_{ij} is the distance between the atoms. The many body nature of the potential is hidden in the bond order parameter $\bar{b}_{ij}$ which is a function of the coordination. Full details of the potential and the parameterisation can be found in Brenner's original paper [38].

Molecular dynamics simulations were performed on infinite length nanotubes making use of periodic boundary conditions and finite length nanotubes terminated by hydrogen atoms. Initial configurations were created by rolling a perfect graphene sheet around a cylinder centred on the z-axis to form a replicable section of tube. H-terminated tubes were created from an infinite zigzag tube by removing the periodic boundaries and adding a hydrogen atom vertically above the highest and below the lowest carbon atoms at a distance of 1.1 Å. To perform the simulations we used our fast serial molecular dynamics software MOLDSIM.†

All simulations were performed in the microcanonical ensemble using the leapfrog Verlet algorithm with a time step of 1 fs. During the equilibrium phase the system was driven down to 5 K using a Berendsen [46] thermostat over a period of 200,000 time steps. When initial velocities were assigned, care was taken to ensure that the total linear and angular momentum of the system was zero. The production run consisted of 164,000 time steps (a convenient number of steps for the FFT procedure) in the microcanonical ensemble. In order to accentuate the RBM, the x and y positions in the initial configuration were scaled to 100.5% of their equilibrium values, thus expanding the tube in the radial direction. For every 10 time steps the average radial distance of the atoms from the z-axis was output to a file. The spectral response was then attained by Fourier transforming these values using a Fast Fourier Transform (FFT) routine to obtain the velocity auto-correlation function $\hat{C}'_{AA}(\upsilon)$,

$$\hat{C}'_{AA}(\upsilon) = \hat{A}^*(\upsilon)\hat{A}(\upsilon) = |\hat{A}(\upsilon)|^2 \tag{4}$$

where υ is the discrete frequency index and $\hat{A}(\upsilon)$ is the Fourier transform of the average radial atomic distance [47]. Using 16,000 points, our spectral resolution was 0.006 THz ($0.2\,\mathrm{cm}^{-1}$). The spectra were further smoothed by using a Blackman–Harris minimum 4-term (sidelobe −92 dB) window function [48].

3. Results and discussion

3.1 Infinite nanotubes

Simulations were carried out for nanotubes of radii ranging 4.7–8.1 Å. Nanotubes typically consisted of around 200 atoms with periodic boundary conditions imposed in the z direction. The RBM was marked, and can be seen clearly from video clips of the simulation. As the radial displacement of the atoms are averaged at each step before they are Fourier transformed, only synchronised radial movement is visible on the spectra, making the radial breathing (monopole) mode very easy to spot. The tubes were particularly sensitive to the amplitude of the radial oscillations; when the displacement exceeded a certain amount (usually above 0.5%), the RBM seemed to couple with other vibrational modes giving two or more peaks centred around (though not directly on) the RBM frequency with certain tubes being more susceptible to coupling than others. Coupling between the RBM and other symmetric vibrational modes has also been considered using *ab initio* techniques by Jeno Kürti *et al.* [19], though the present research suggests that coupling between different modes is more common that was previously thought and leads to a shifting of the RBM frequency. This behaviour is in itself quite interesting, but is not the subject of this paper, though animations of

†MOLDSIM is a molecular dynamics simulation package written in C++ by Matthew Longhurst, Imperial College. For more information see www.MOLDSIM.com.

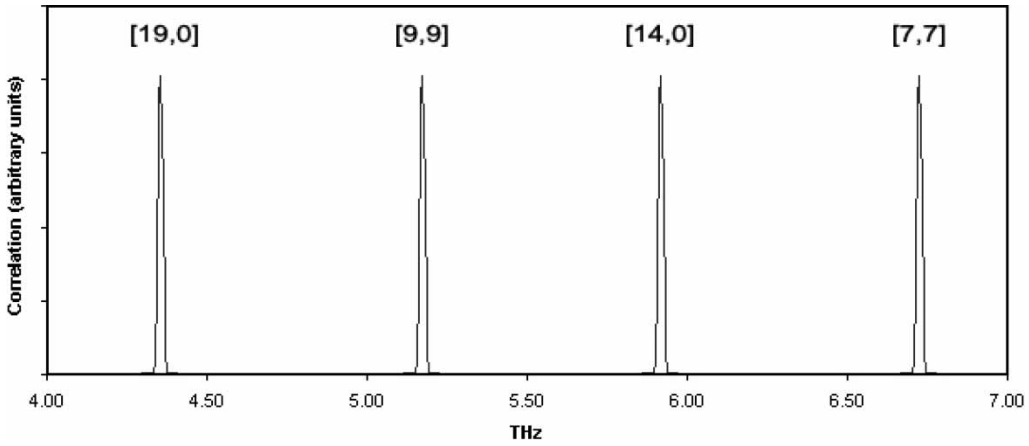

Figure 1. Typical spectra for four nanotubes of different radii. Only one peak is visible representing the RBM frequency. The spectral resolution is 0.006 THz.

coupling can be seen on the Molecular Simulation website, http://www.tandf.co.uk/journals/titles/08927022.asp. In order to maintain a pure RBM, initial radial expansions of less than 0.5% were usually necessary. This figure is significantly lower than that used in other studies [19,34].

Figure 1 shows some typical spectra ([7,7], [14,0], [9,9], and [19,0] nanotubes). The peaks are very clear, and under close examination appear to be Gaussian, indicating that even at such a low initial expansion, the RBM is not perfectly harmonic. The full results for the RBM frequencies can be seen in table 1 where they are compared to other available data (original Tersoff-Brenner bond order potential (BOP) [34], tight binding (TB) [25,26], *ab initio* calculations [19,18], force field [44] and assignment of low frequency Raman modes [45,16]). As expected, the frequency of the RBM is inversely proportional to the nanotube radius; figure 2A plots RBM frequency against $1/R_0$, where R_0 is the nanotube radius and figure 2B plots RBM period against R_0. Note that we found two different linear fits to the data, one for zigzag tubes and one for armchair tubes. The frequencies were fitted to α/R_0 with $\alpha = 3.18$ THz nm for armchair tubes and 3.25 THz nm for zigzag tubes as compared to $\alpha = 3.35$ THz nm as a general fit to all points with our previous potential [34] (though a much better fit was found using a y intercept of -0.2 THz suggesting the $1/R_0$ rule does not hold exactly for all lengths). When the RBM *period* is plotted against nanotube radius (figure 2B), the armchair fit lies parallel to about 4 fs above the zigzag fit. A difference in RBM period for armchair tubes as compared to zigzag tubes should perhaps be expected given the different topologies of the nanotubes; in armchair tubes some C—C bonds lay parallel to the direction of expansion, whereas in zigzag tubes all the C—C bonds lay at an angle. Differences in the Young's modulus between zigzag and armchair tubes have already been observed by Wang *et al.* using this same potential [49]. It is worth noting that this potential seems to underestimate the RBM frequencies as compared to other published results by approximately 3–7%.

3.2 Finite nanotubes

The starting point for the finite tube simulations was to use the zigzag tubes from the infinite tube study, remove

Table 1. Comparison of RBM frequencies of SWNT calculated using REBO potential (this paper), original Tersoff-Brenner BOP, TB, *ab initio* calculations, force field, and assignment of low frequency Raman modes (frequencies in THz).

	R_0/Å	REBO	BOP q-[34]	TB [25,26]		*Ab initio* [18,19]		FF [44]	Experiment [45,16]	
[7,7]	4.766	6.73	6.98	8.04		7.38			6.90	7.35
[13,0]	5.118	6.42	6.50	7.41					6.33	
[8,8]	5.446	5.84	6.12	7.14	5.91	6.49	6.40	6.18	6.18	
[14,0]	5.506	5.91	6.04			6.37			5.85	
[15,0]	5.896	5.52	5.65	6.42		5.89			5.70	5.97
[9,9]	6.117	5.19	5.44	6.42	5.25	5.78		5.49	5.46	
[16,0]	6.284	5.17	5.28			5.59			5.31	
[17,0]	6.672	4.86	4.92		4.80	5.26			5.01	
[10,10]	6.791	4.68	4.85	5.85	4.71	5.20	4.70	4.95	4.86	
[18,0]	7.051	4.57				4.93				
[19,0]	7.450	4.32	4.57			;4.72				
[11,11]	7.462	4.24	4.76	5.34		4.74		4.5	4.68	
[20,0]	7.840	4.09	4.45	4.98		4.48			4.41	
[12,12]	8.142	3.86	4.03	4.92				4.38		

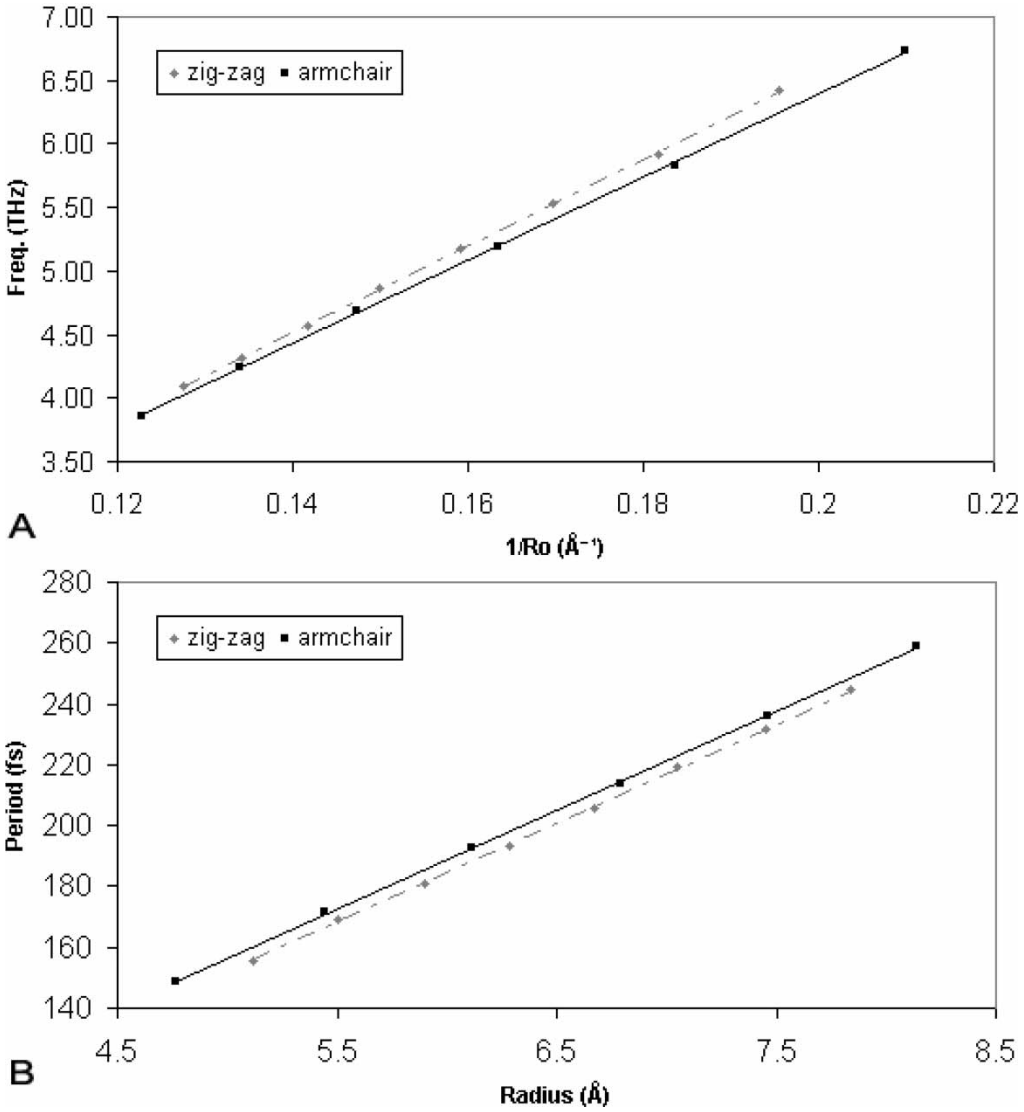

Figure 2. (A) RBM frequency plotted against $1/R_0$ where R_0 is the nanotube radius. (B) RBM period plotted against nanotube radius. Dot-dash – zigzag tubes, solid line – armchair tubes.

the periodic boundary conditions in the z direction and terminate them with hydrogen atoms. The lengths of shortest and longest nanotubes used were 1.7 and 13.642 nm, respectively. For the [19,0] tube, a more extensive study was carried out with 20 different measurements of the RBM between nanotubes of lengths 1.7 and 27.2 nm. Simulations were carried out in an identical way to the infinite tube simulations. figure 3 shows a ball and stick representation of a [13,0] H-terminated nanotube brought to equilibrium at 5 K, and a schematic of the tube termination. As can be seen, the hydrogens orientate themselves in the outwards direction. This angle was calculated to be 16.56° and the C—H bond length was 1.08 Å.

The spectra produced are not as clean as the spectra for the infinite tubes due to end effects. With the smaller tubes, one or two close peaks are seen, while with the larger tubes there is usually one peak surrounded by a region of noise. From this point on, we will define the RBM frequency as the average frequency of the peak(s) corresponding to radial movement. We will also define the error δ as the frequency spread of these peaks or the corresponding noise. The finite tube results for four different nanotube lengths can be seen in table 2, while figure 4 plots the RBM frequency for a [19,0] nanotube at 20 different lengths. As can be seen, the RBM quickly approaches the infinite length value for nanotubes greater than 5 nm in length. This result is reassuring as it removes one of the assumptions often made in molecular simulations. For lengths under 5 nm, the RBM frequency increases exponentially. In fact, closer examination of the spectra for the shortest tube reveals that the RBM is not the dominant mode. Two or three taller peaks are visible around the 3–4 THz range which, from examination of the video clips, seem to correspond to higher radial modes and general complexity associated with the terminated ends. Finally, the radial vibrational frequency of the terminating hydrogen atoms was calculated by freezing all of the carbon atoms and expanding the hydrogen atoms 0.5% in

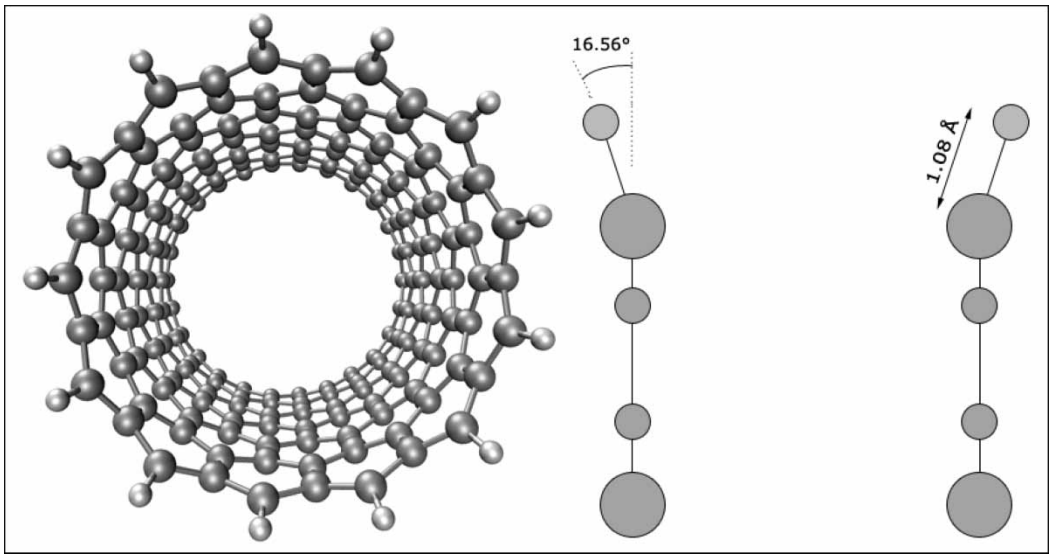

Figure 3. Left: Ball and stick representation of H-terminated nanotube at equilibrium. Image created by VMD‡ and rendered by POV-Ray.¶ Right: Schematic of H termination with bond length and angle.

Table 2. RBM frequencies for finite length zigzag tubes of different radius (four different lengths of nanotubes are specified and δ represents the spread of the peak(s); frequencies in THz).

	R_0/Å	RBM-infinite	RBM (δ)			
			1.705 nm	3.410 nm	6.821 nm	13.642 nm
[13,0]	5.118	6.42	7.21 (0.46)	6.45 (0.03)	6.40 (0.11)	6.41 (0.07)
[14,0]	5.506	5.91	6.90 (0.63)	5.98 (0.18)	6.00 (0.38)	5.90 (0.30)
[15,0]	5.896	5.52	7.08 (0.05)	5.61 (0.13)	5.53 (0.12)	5.52 (0.12)
[16,0]	6.284	5.15	7.00 (0.05)	4.98 (0.57)	5.19 (0.08)	5.16 (0.16)
[17,0]	6.672	4.83	6.93 (0.06)	4.96 (0.10)	4.85 (0.12)	4.84 (0.18)
[18,0]	7.051	4.57	6.89 (0.05)	4.71 (0.03)	4.57 (0.03)	4.57 (0.05)
[19,0]	7.450	4.32	6.84 (0.06)	4.49 (0.06)	4.33 (0.03)	4.33 (0.13)

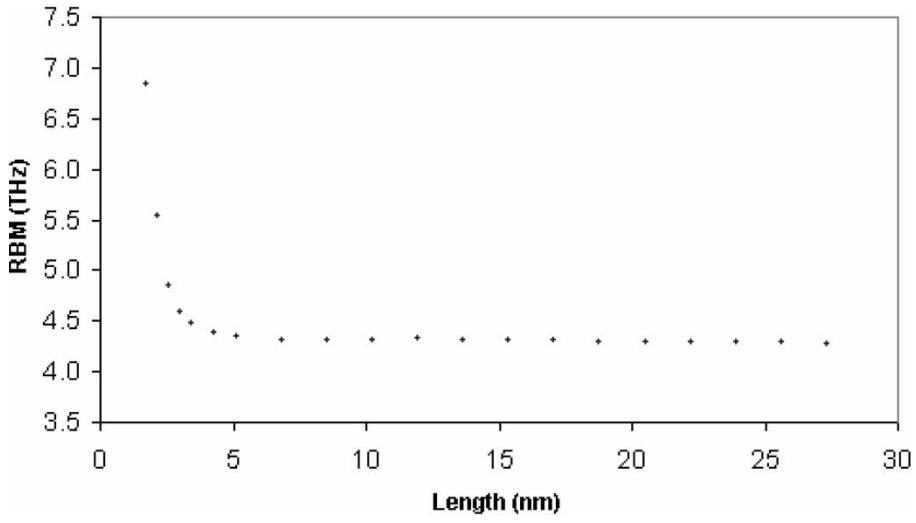

Figure 4. RBM frequencies for finite length [19,0] nanotube. Above 5 nm, the RBM frequency quickly approaches that of the infinite tube.

‡VMD is a free molecular visualisation program developed by the Theoretical and Computational Biophysics group of the University of Illinois—http://www.ks.uiuc.edu/Research/vmd/.

¶POV-Ray is a free ray tracing tool—www.povray.org.

the radial direction. The "radial breathing", or out of plane movement of the hydrogen atoms was then measured using the same technique used to calculate the RBM except that a time step of 0.1 fs was used. The hydrogen radial frequency was found to be 85.7 THz, independent of nanotube radius.

4. Conclusions

Using molecular dynamics, we have calculated the RBM frequencies of a range of infinite and finite length SWCNTs using the second generation REBO potential. Our technique gives a spectral resolution of 0.006 THz. The RBM frequencies were fitted to α/R_0 with $\alpha = 3.18\,\text{THz nm}$ for armchair tubes and 3.25 THz nm for zigzag tubes. Finite length tubes were created from zigzag tubes by removing periodic boundaries and terminating dangling bonds with hydrogen atoms. The hydrogen atoms were found to orientate themselves in an outward direction at 16.56°, and the C—H bond length was measured at 1.08 Å. The RBM frequency for tubes with lengths greater than 5 nm quickly approached the infinite RBM frequency, whereas the RBM frequency for tubes lesser than 5 nm increased exponentially. Finally, the radial vibrational frequency of the terminating hydrogen atoms was found to be 85.7 THz, independent of nanotube radius.

Acknowledgements

M J Longhurst thanks the National Physical Laboratory, Teddington UK for a CASE award.

References

[1] C. Journet, W.K. Maser, P. Bernier, A. Loiseau, M.L. DelaChapelle, S. Lefrant, P. Deniard, R. Lee, J.E. Fischer. Large-scale production of single-walled carbon nanotubes by the electric-arc technique. *Nature*, **388**, 756 (1997).

[2] R. Saito, G. Dresselhaus, M.S. Dresselhaus. *Physical Properties of Carbon Nanotubes*, ICP, London (1998).

[3] K. Tohji, M. Sugano, A. Kasuya, Y. Nishina, Y. Saito, H. Takahashi. Resonant Raman scattering from single-walled nanotubes of small diameters. *Appl. Surf. Sci.*, **144–145**, 657 (1999).

[4] S.C. Tsang, Y.K. Chen, P.J.F. Harris, M.L.H. Green. A simple chemical method of opening and filling carbon nanotubes. *Nature*, **372**, 159 (1994).

[5] M. Freemantle. Blossoming of dendrimers. *Chem. Eng. News*, **77**, 27 (1999).

[6] G. Beni, M.A. Tenan. Dynamics of electrowetting displays. *J. Appl. Phys.*, **52**, 6011 (1981).

[7] B.S. Gallardo, *et al.* Liquids on submillimeter scales. *Science*, **283**, 57 (1999).

[8] S. Supple, N. Quirke. Rapid imbibition of fluids in carbon nanotubes. *Phys. Rev. Lett.*, **90**, 214501 (2003).

[9] H. Rafil-Tabar. Computational modelling of thermo-mechanical and transport properties of carbon nanotubes. *Phys. Rep.*, **390**, 235 (2004).

[10] see for example M.S. Strano, M. Zheng, A. Jagota, G.B. Onoa, D.A. Heller, P.W. Barone, M.L. Usrey. Understanding the nature of the DNA assisted separation of single walled nanotubes using fluorescence and Raman spectroscopy. *Nanoletters*, **4**, 543 (2004).

[11] A.M. Rao, E. Richter, S. Bandow, B. Chase, P.C. Eklund, K.A. Williams, S. Fang, K.R. Subbaswamy, M. Menon, A. Thess, R.E. Smalley, G. Dresselhaus, M.S. Dresselhaus. Diameter-selective Raman scattering from vibrational modes in carbon nanotubes. *Science*, **275**, 187 (1997).

[12] U.D. Venkateswaran, A.M. Rao, E. Richter, M. Menon, A. Rinzler, R.E. Smalley, P.C. Eklund. Probing the single-wall carbon nanotube bundle: Raman scattering under high pressure. *Phys. Rev. B*, **59**, 10928 (1999).

[13] A. Kasuya, Y. Sasaki, Y. Saito, K. Tohji, Y. Nishina. Evidence for size-dependent discrete dispersions in single-wall nanotubes. *Phys. Rev. Lett.*, **78**, 4434 (1997).

[14] A. Kasuya, M. Sugano, T. Maeda, Y. Saito, K. Tohji, H. Takahashi, Y. Sasaki, M. Fukushima, Y. Nishina, C. Horie. Resonant Raman scattering and the zone-folded electronic structure in single-wall nanotubes. *Phys. Rev. B*, **57**, 4999 (1998).

[15] H. Kuzmany, B. Burger, M. Hulman, J. Kürti, A.G. Rinzler, R.E. Smalley. Spectroscopic analysis of different types of single-wall carbon nanotubes. *Europhys. Lett.*, **44**, 518 (1998).

[16] M.S. Strano, S.K. Doorn, E.H. Haroz, C. Kittrell, R.H. Hauge, R.E. Smalley. Assignment of (n,m) Raman and optical features of metallic single-walled carbon nanotubes. *Nano Lett.*, **3**, 1091 (2003).

[17] U. Kuhlmann, H. Jantoljak, N. Pfander, P. Bernier, C. Journet, C. Thomsen. Infrared active phonons in single-walled carbon nanotubes. *Chem. Phys. Lett.*, **294**, 237 (1998).

[18] D. Sánchez-Portal, E. Artacho, J.M. Soler, A. Rubio, P. Ordejón. *Ab-initio* structural, elastic and vibrational properties of carbon nanotubes. *Phys. Rev. B*, **59**, 12678 (1999).

[19] J. Kürti, V. Zólyomi, M. Kertesz, G. Sun. The geometry and the radial breathing mode of carbon nanotubes: beyond the ideal behaviour. *New J. Phys.*, **5**, 125 (2003).

[20] J. Yu, R.K. Kalia, P. Vashishta. Phonons in graphitic tubules—a tight-binding molecular-dynamics study. *J. Chem. Phys.*, **103**, 6697 (1995).

[21] E. Richter, K.R. Subbaswamy. Theory of size-dependent resonance Raman scattering from carbon nanotubes. *Phys. Rev. Lett.*, **79**, 2738 (1997).

[22] R. Saito, T. Takeya, T. Kimura, G. Dresselhaus, M.S. Dresselhaus. Raman intensity of single-wall carbon nanotubes. *Phys. Rev. B*, **57**, 4145 (1998).

[23] R. Saito, T. Takeya, T. Kimura, G. Dresselhaus, M.S. Dresselhaus. Raman intensity of single-wall carbon nanotubes. *Phys. Rev. B*, **59**, 2388 (1999).

[24] T. Maeda, C. Horie. Phonon modes in single-wall nanotubes with a small diameter. *Physica B*, **263–264**, 479 (1999).

[25] D. Kahn, J.P. Lu. Vibrational modes of carbon nanotubes and nanoropes. *Phys. Rev. B*, **60**, 6535 (1999).

[26] L. Henrard, E. Hernándes, P. Bernier, A. Rubio. van der Waals interaction in nanotube bundles: consequences on vibrational modes. *Phys. Rev. B*, **60**, R8521 (1999).

[27] R.A. Jishi, L. Venkataraman, M.L. Dresselhaus, G. Dresselhaus. Phonon modes in carbon nanotubules. *Chem. Phys. Lett.*, **209**, 77 (1993).

[28] S. Erkoc. Empirical many-body potential energy functions used in computer simulations of condensed matter properties. *Phys. Rep.*, **278**, 80 (1997).

[29] G.C. Abell. Empirical chemical pseudopotential theory of molecular and metallic bonding. *Phys. Rev. B*, **31**, 6184 (1985).

[30] J. Tersoff. New empirical model for the structural properties of silicon. *Phys. Rev. Lett.*, **56**, 632 (1986).

[31] J. Tersoff. New empirical approach for the structure and energy of covalent systems. *Phys. Rev. B*, **37**, 6991 (1988).

[32] J. Tersoff. Empirical interatomic potential for carbon, with applications to amorphous carbon. *Phys. Rev. Lett.*, **61**, 2879 (1988).

[33] D.W. Brenner. Empirical potential for hydrocarbons for use in simulating the chemical vapor deposition of diamond films. *Phys. Rev. B*, **42**, 9458 (1990).

[34] V.P. Sokhan, D. Nicholson, N. Quirke. Phonon spectra in model carbon nanotubes. *J. Chem. Phys.*, **113**, 2007 (2000).

[35] V.P. Sokhan, D. Nicholson, N. Quirke. Transport properties of nitrogen in single walled carbon nanotubes. *J. Chem. Phys.*, **120**, 3855 (2004).

[36] S. Supple, N. Quirke. Molecular dynamics of transient oil flows in nanopores 1: imbibition speeds for single wall carbon nanotubes. *J. Chem. Phys.*, **121**, 8571 (2004).

[37] V.P. Sokhan, D. Nicholson, N. Quirke. Fluid flow in nanopores: accurate boundary conditions for carbon nanotubes. *J. Chem. Phys.*, **117**, 8531 (2002).
[38] D.W. Brenner, O.A. Shenderova, J.A. Harrison, S.J. Stuart, B. Ni, S.B. Sinnott. A second-generation reactive empirical bond order (REBO) potential energy expression for hydrocarbons. *J. Phys.: Condens. Matter*, **14**, 783 (2002).
[39] J.A. Harrison, S.J. Stuart, D.H. Robertson, C.T. White. Properties of capped nanotubes when used as SPM tips. *J. Phys. Chem. B*, **101**, 9682 (1997).
[40] A. Garg, J. Han, S.B. Sinnott. Interactions of carbon-nanotubule proximal probe tips with diamond and graphene. *Phys. Rev. Lett.*, **81**, 2260 (1998).
[41] A. Garg, S.B. Sinnott. Effect of chemical functionalization on the mechanical properties of carbon nanotubes. *Chem. Phys. Lett.*, **295**, 273 (1998).
[42] Z. Mao, A. Garg, S.B. Sinnott. Molecular dynamics simulations of the filling and decorating of carbon nanotubules. *Nanotechnology*, **10**, 273 (1999).
[43] D. Srivastava, D.W. Brenner, J.D. Schall, K.D. Ausman, M.F. Yu, R.S. Ruoff. Predictions of enhanced chemical reactivity at regions of local conformational strain on carbon nanotubes: Kinky chemistry. *J. Phys. Chem. B*, **103**, 4330 (1999).
[44] A.M. Rao, E. Richter, S. Bandow, B. Chase, P.C. Eklund, K.A. Williams, S. Fang, K.R. Subbaswamy, M. Menon, A. Thess, R.E. Smalley, G. Dresselhaus, M.S. Dresselhaus. Diameter-selective Raman scattering from vibrational modes in carbon nanotubes. *Science*, **275**, 187 (1997).
[45] H. Kuzmany, B. Burger, M. Hulman, J. Kürti, A.G. Rinzler, R.E. Smalley. Spectroscopic analysis of different types of single-wall carbon nanotubes. *Europhys. Lett.*, **44**, 518 (1998).
[46] H.J. Berendsen, J.P. Postma, A. DiNola, J.R. Haak. Molecular-dynamics with coupling to an external bath. *J. Chem. Phys.*, **81**, 3684 (1984).
[47] M.P. Allen, D.J. Tildesley. *Computer Simulation of Liquids*, **190**, Oxford Science Publications (1987).
[48] F.J. Harris. On the use of windows for harmonic analysis with the discrete Fourier transformation. *Proc. IEEE*, **66**, 51 (1972).
[49] Y. Wang, X.X. Wang, X.G. Ni, H.A. Wu. Buckling behavior of carbon nanotube under compression. *Acta Physica Sinica*, **52**, 3120 (2003).